Field test of the accuracy of laser particle counters to measure aeolian sediment flux

Duarte-Campos, Leonardo; Wijnberg, Kathelijne M.; Hulscher, Suzanne J.M.H.

DOI
10.1016/j.aeolia.2021.100676

Publication date
2021

Document Version
Final published version

Published in
Aeolian Research

Aeolian Research 50 (2021) 100676

Contents lists available at ScienceDirect

Aeolian Research

journal homepage: www.elsevier.com/locate/aeolia

Field test of the accuracy of laser particle counters to measure aeolian sediment flux

Leonardo Duarte-Campos [a,b,*], Kathelijne M. Wijnberg [a], Suzanne J.M.H. Hulscher [a]

[a] Water Engineering and Management, Faculty Engineering Technology, University of Twente, P.O. Box 217, 7500AE Enschede, The Netherlands
[b] Current address: Department of Hydraulic Engineering, Faculty of Civil Engineering and Geosciences, Delft University of Technology, P.O. Box 5048, 2600GA Delft, The Netherlands

ARTICLE INFO

Keywords:
Aeolian sand transport
Wenglor
Sand trap
Grain size
Transport measurement

ABSTRACT

In this study we tested to what extent grain count data from a laser particle counter, when enriched with granulometric data, can lead to accurate measurements of aeolian sediment fluxes in the field. Field experiments were conducted at Koksijde beach (Belgium) with a vertical array of five Wenglor fork sensors and co-located vertically stacked mesh sand traps. Sand collected in the traps was used to both obtain the reference values for sediment flux as well as to obtain granulometric data at the five Wenglor sensor elevations. Grain counts were transformed to sediment fluxes by combining the granulometric data with the grain size dependent, effective detection width concept. It was found that the limitation of the Wenglor sensor to have a minimum detectable grain size, well within the diameter range of sand grains in transport, could easily be corrected for through a linear relation of Wenglor detectable sediment flux with total sediment flux. However, we found that the Wenglor derived fluxes deviated from the sand trap derived fluxes in an inconsistent manner, both in the vertical and over time, which made us conclude that there is no uniform calibration possible to match the Wenglor data with the trap data. This suggests that further studies using optical aeolian transport sensors should focus on analysing the raw photoelectric signal rather than on internally processed count data.

1. Introduction

Aeolian sand transport is being measured for quite some time now. The first experiments and results were presented by Bagnold (1936). In 1938, he introduced his trap (Bagnold, 1938) as the first attempt to measure and quantify aeolian sand transport by using a special device. During the last 80 years several instruments have been developed, trying to improve the efficiency of the measurements. The instruments or devices to measure aeolian sand transport can be described in three main groups, according to their measurement principles: *Sand traps* (Leatherman, 1978; Arens and van der Lee, 1995; Sherman et al., 2014; Hilton et al., 2017), *Impact sensors* (Baas, 2004; de Winter et al., 2018; Ellis et al., 2009; Rezaei et al., 2020) and *Optical sensors* (Duarte-Campos et al., 2017; Etyemezian et al., 2017; Hugenholtz and Barchyn, 2011). Several studies have compared the different kinds of instruments of a same group (van Pelt et al., 2009; Poortinga et al., 2015). Other studies have combined devices from different groups to measure aeolian sand transport and also to compare or calibrate these instruments that work according to different principles (Sherman et al., 2011; Goossens et al., 2000; Davidson-Arnott et al., 2009; Yurk et al., 2013; Goossens et al., 2018).

Each instrument or sensor has its strengths and weaknesses. For instance, an optical sensor, like the Wenglor (Sherman et al., 2011; Hugenholtz and Barchyn, 2011; Delgado-Fernandez et al., 2012), can give us detailed data in terms of transport variations on a time scale of seconds, but by using this optical sensor we will know only the number of sand grains that cross the laser beam. If the goal is to obtain data on fluxes of aeolian sand transport, the Wenglor data needs to be enriched with information about the grain size distribution of the sand that crosses the Wenglor beam area (Barchyn et al., 2014; Duarte-Campos et al., 2017). Alternatively, by using sand traps it is possible to know the average flux over a specific period of time of minutes to hours, as well as the particle size distribution of the grains transported by the wind, but we lose all the information on temporal variability of the transport during the sand collection period.

During the last decade, Wenglor sensors have been used in several

* Corresponding author at: Department of Hydraulic Engineering, Faculty of Civil Engineering and Geosciences, Delft University of Technology, P.O. Box 5048, 2600GA Delft, The Netherlands.
E-mail address: leonardo.duartec@gmail.com (L. Duarte-Campos).

https://doi.org/10.1016/j.aeolia.2021.100676
Received 26 May 2020; Received in revised form 28 December 2020; Accepted 12 January 2021
Available online 5 February 2021

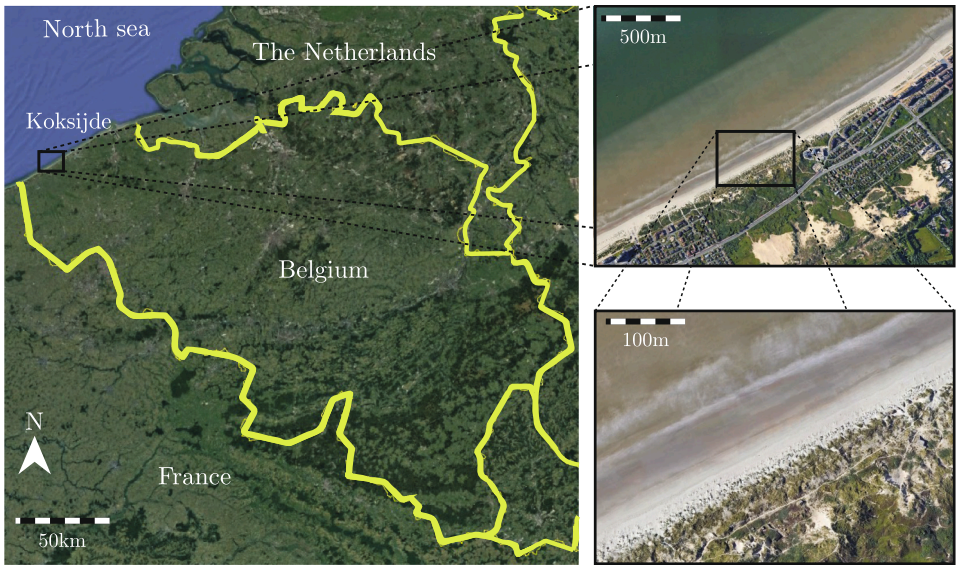

Fig. 1. Study area and its location in the Belgian coast.

fieldwork deployments with different purposes and wind conditions. For example, Bauer and Davidson-Arnott (2014) utilized Wenglor sensors during a storm at Prince Edward Island National Park (Canada); focussing their analysis on a period of intense sand transport that lasted 3 h. In this experiment the Wenglor data, collected at 1 Hz, was divided in intervals of 15 min to determine vertical profiles of particle flux and the variations of this vertical distribution over time. Hoonhout and de Vries (2017) present the results of several days of experiments using spatial transects of vertically stacked Wenglor sensors at The Sand Motor (The Netherlands). The data collected was divided in subsets of several hours in which count data gathered at 1 Hz was summed over the vertical and averaged over periods of one hour, to determine spatial variations in aeolian sediment availability from the intertidal beach towards the dunes.

The aim of this paper is to test to what extent enriching grain count data with granulometric data from co-located sand traps can lead to accurate measurements of aeolian sand fluxes using the Wenglor sensor. Taking into account the recent insight that the Wenglor sensor can detect only grains larger than 210 μm (Duarte-Campos et al., 2017), we will also assess to what extent this forms a limitation to derive total sediments flux.

We present the results of field experiments in which we compare and quantify the saltation fluxes of aeolian sand transport, using co-located vertical arrays of a laser particle counter (Wenglor) and vertically stacked mesh sand traps.

This paper is organized as follows. In Section 2, the study area is described. In Section 3 the instrumentation used at the field is presented. Section 4 and Section 5 shows the conducted experiments and the results, respectively. In Section 6, the discussion is presented. Finally, in Section 7 a summary and the main conclusions of this study are presented.

2. Study area

Field experiments of aeolian sand transport were conducted at Koksijde beach (Belgium), located on the southwest Belgian coast (Fig. 1), close to the French border. Koksijde beach is a natural sandy beach (D_{50} of approximately 220 μm) and is located in a (ultra) dissipative macrotidal environment, with a South West - North East orientation (Speybroeck et al., 2008). The intertidal zone has a slope around 1% and is characterized by ridge and runnels topography (Speybroeck et al., 2008; Voulgaris et al., 1998). Tides in this area are semi-diurnal

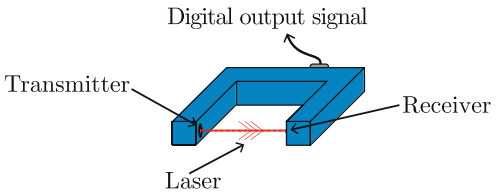

Fig. 2. Laser particle counter, also known as Wenglor.

with a large neap to spring variation, 3.5 to 5 m respectively (Haerens et al., 2012). During neap low tide, the sand bank Broersbank is visible and acts as a natural island in front of the coastline (Strypsteen et al., 2017). The intertidal beach width ranges between 250–500 m (Voulgaris et al., 1998). Wind and waves direction are mainly from the South West to North West and the typical wave height is about 0.5–1 m (Haerens et al., 2012). The dominant southwesterly winds also induce a north-eastern aeolian drift (Speybroeck et al., 2008). The supratidal beach is approximately 30 m wide. The experiments were carried out at the transition of the intertidal beach with the upper beach, in a zone free of groins where dunes are the upper boundary of the beach. The experiments were conducted on November 24, 2016.

3. Instrumentation

3.1. Laser particle counter Wenglor

Saltating grains were counted using Wenglor photoelectronic sensors at five elevations, between 0.04 m and 0.26 m. This sensor has a laser beam travelling from a transmitter to a receiver (Fig. 2) and as been used in several aeolian sand transport studies, both in the field and in wind tunnel experiments and its characteristics are well known (Sherman et al., 2011; Hugenholtz and Barchyn, 2011).

Duarte-Campos et al. (2017) showed that the intensity of the Wenglor laser beam is not uniformly distributed over its cross-section and increases towards the center of the laser beam. This implies that the area in which a particle crosses the laser beam is important to achieve a count and also that smaller detectable particles will have a larger chance to be counted if they pass through the center of the laser beam.

The non-uniform intensity distribution of the Wenglor laser beam leads to the effective detection width (EDW) definition, which corresponds to the diameter of the area in which the center of a particle can

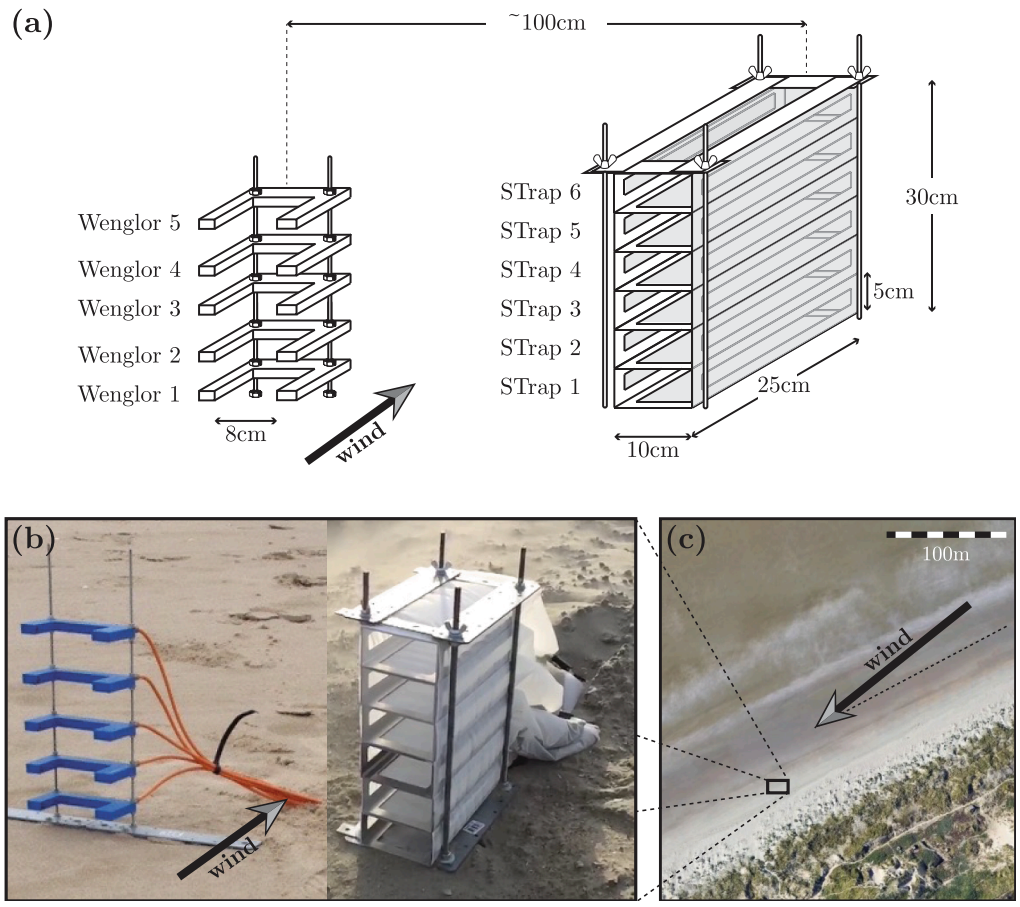

Fig. 3. a) Sketch of the vertical array of Wenglor sensors and sand traps, with their main dimensions. b) Wenglor sensor array and sand traps deployed at the beach surface. c) Location of the instruments at the beach. For all the figures the wind direction is indicated.

move through the laser beam to result in a count (Duarte-Campos et al., 2017). This area increases with the particle diameter and for particles of 210 μm (smallest detectable particle) the EDW is zero, i.e. these particles will be detected only if their centers pass through the center of the laser beam. Duarte-Campos et al. (2017) fitted a second degree polynomial to the measured laser intensity variation, over the cross-section of the beam, to obtain a direct relation between grain size and laser intensity reduction, which is summarized in their figure 14a. It is important to emphasize that EDW has been defined and calculated for spherical particles.

Previous studies have tested three versions of the Wenglor sensor: the YH08PCT8 (80 mm fork width) (e.g., Bauer and Davidson-Arnott, 2014), the YH05PCT8 (50 mm fork width) (e.g., Goossens et al., 2018), and the YH03PCT8 (30 mm fork width) (e.g., Hugenholtz and Barchyn, 2011). The only difference between them is the fork width, or the distance between the transmitter and the receiver (Fig. 2). Smaller sampling areas record more intermittent transport, whilst larger sampling areas record smoother data (Barchyn et al., 2014). Despite their identical electronic design, the listed sensors could behave differently during intense transport period. Bauer et al. (2018) recommend to deploy 30 mm sensors when large flux rates are anticipated, and the 80 mm sensor at high elevations in the vertical flux profile or during intermitent transport. However, a correct sampling area does not exist and each sampling area provides different view of the aeolian sand transport (Barchyn et al., 2014).

We use Wenglor sensors with a fork width of 80 mm (Wenglor fork sensor YH08PCT8), which from now on will be referred to as Wenglor sensor. During the measurements, Wenglor sensors were set on Normally Open and Minimal teach-in setting. The "teach-in" step is a self-calibration procedure that determines at which level of reduction of the photoelectric signal the sensor produces a count (Hugenholtz and Barchyn, 2011).

3.2. Sand traps

Simultaneous to the Wenglor count measurements, co-located vertically stacked mesh sand traps (Fig. 3) were used to collect sand over fixed time intervals at various elevations. The array consists of 6 traps that in total cover 30 cm in height. Trap frames were fabricated from aluminium following the design proposed by Sherman et al. (2014). Each trap frame is 10 cm wide, 25 cm long, 5 cm high and the edges are 2 mm thick. To allow the sand collection each trap frame was covered with a bag made from "nylon mono filament" with 40 μm filament diameter and 50 μm mesh size. The nylon bags were longer than the trap frame, that means that the sand grains can pass through the frame and then accumulated outside of the frame. For the bottom trap a bag of 75 cm long (including the frame) was used and for all the other the bag was 50 cm long. Bags were closed using binder clips, and the traps array was stacked with bracket of threaded rod. Fig. 3 shows a deployment of the vertical array of traps at the beach surface. As can be seen, the sand has accumulated at the end of the nylon bag, out of the trap frame.

Sherman et al. (2014) state that depending on the transport rates, this sand trap is highly efficient when it is used in short term measurements (periods of tens of minutes or less). Additionally, Hilton et al. (2017) show that the efficiency of the mesh trap is comparable to their self-orienting trap. The results presented by Strypsteen et al. (2020) show that the mesh trap collects between 5% to 10% less than the amount of sand collected with Modified Wilson and Cook (MWAC) sand traps (Sterk and Raats, 1996).

Table 1
Duration of conducted runs in seconds and average wind speed at 0.5 m above the ground.

Run	1	2	3	4	5	6	7	8	9
Duration (s)	2200	2040	960	1051	1440	1080	1440	1320	2249
WS (m/s)	7.2	8.5	8.4	8.7	9.2	9.2	9.1	9.2	9.2

Table 2
Wenglor sensor elevations in meters.

	Wenglor 1	Wenglor 2	Wenglor 3	Wenglor 4	Wenglor 5
Height (m)	0.04	0.09	0.15	0.20	0.26

4. Field Experiments

To validate the performance of the Wenglor sensor during field deployments with respect to recording fluxes of sand grains above the detection limit, i.e. 210 μm, we co-located a vertical array of Wenglor sensors and vertical stacked sand traps on the beach. As the information from traps and optical sensor is complementary to some extent, fluxes obtained from sand traps measurements will be used as representative for further comparison with the fluxes obtained from Wenglor measurements. This is in accordance with the calibration methodology proposed by Martin et al. (2018).

The sand collection using sand traps was carried out nine times. The duration of each deployment (run) of the trap array varied as presented in Table 1. At the end of each run, the array of sand traps was removed and a new, i.e. sand-free, trap array was located in the same position to start a new sand collection experiment. The Wenglor sensors were connected to a *Hobo Energy Logger*, to record the counts (1 Hz acquisition rate) that the sand grains produce when they cross through the laser beam. The data collection period covered approximately 5 h, from 11:00 AM till the end of the deployments at 4:00 PM. Then the data was split in 9 subsets according to the sand collection interval of the sand traps. The teach-in procedure (minimal teach-in) of the sensor was applied once, before the start of the runs. The location of the vertical arrays of Wenglor sensors and sand traps were fixed, and were aligned perpendicular to the prevailing wind direction.

The average wind speed, measured with a cup anemometer at 0.50 m above the surface, ranged between 7.2 and 9.2 m/s from the beginning until the end of the deployments (Table 1) (Glenn Strypsteen, personal communication, December 13, 2016; and Strypsteen et al., 2017). During the day of the experiments, the wind direction was almost constant and highly oblique onshore, with an average value of 70 degrees northeast, i.e. 8 degrees out of longshore direction (Strypsteen, 2019).

As explained in Section 3.1, the Wenglor sensor can detect only individual particles larger than 210 μm. Hence, for every sand sample the weight of all the grains under this limit must be removed to obtain a new sample mass, $M^{>210}$ that forms a fair comparison for what the sensor can observe. Because the Wenglor sensor array only measured saltation transport (Table 2), a fair comparison to the trap data should exclude the bottom trap data, due to the fact that this trap catches sand grains from saltation and reptation or creep modes. Specifically the latter mode will not be detected by the Wenglor sensor located at 4 cm above the surface causing a probable mismatch between sand trap and Wenglor.

The mass collected by each trap ($M^{>210}$) has to be converted to flux using the effective trap area (A = width × height) equal to $46 \times 96 \times 10^{-6}\mathrm{m}^2$ and its respective experiment duration, presented in Table 1. Then, the flux obtained must be associated to a representative elevation to characterize the vertical distribution and to allow the comparison with the measurements from the Wenglor sensors at different elevations. Ellis et al. (2009) state that the geometric mean elevation is physically more representative of the non-linear distribution of flux above the bed. Several studies have shown that the vertical distribution of mass flux is best described using an exponential decay curve $q(z)=\alpha exp(\beta z)$ (Ellis et al., 2009; Rotnicka, 2013; Bauer and Davidson-Arnott, 2014; Strypsteen et al., 2020), where $z = \sqrt{h_{\mathrm{top}} \times h_{\mathrm{bottom}}}$, corresponds to the geometric mean elevation of the respective trap (Ellis et al., 2009; Rotnicka, 2013). The geometric mean elevation (in meters), for our experiments, of each trap is presented in Table 3.

Table 3
Geometric mean elevation ($z = \sqrt{h_{\mathrm{top}} \times h_{\mathrm{bottom}}}$,) for each Trap. Values are expressed in meters.

	Trap 2	Trap 3	Trap 4	Trap 5	Trap 6
Geometric Mean (m)	0.07	0.12	0.17	0.22	0.27

Once the vertical flux distribution for the sand trap measurements is obtained, the next step is to transform the Wenglor count data into fluxes as well. For this, we use the equation proposed by (Barchyn et al., 2014), but modified according to the EDW concept (Section 3.1). Including the EDW the equation is:

$$\frac{q_{\mathrm{w}}}{n_{\mathrm{w}}} = \left(\frac{24\, l_{\mathrm{f}}}{\rho \pi} \sum_{j} \frac{\gamma_j \left(\mathrm{EDW}_j + D_j + \mathrm{EDW}_{j+1} + D_{j+1} \right)}{\left(D_j + D_{j+1} \right)^3} \right)^{-1} \tag{1}$$

Where q_{w} is the mass flux (kg/m^{2}s) for each Wenglor, n_{w} correspond to the counts/s gathered with the Wenglor sensor, D_j and D_{j+1} the boundaries of the grain size class considered with its respective mass proportion (γ_j) obtained in the grain size analysis; l_{f} is the fork width of the sensor (0.08 m), EDW_j correspond to the effective detection width of a particle with diameter D_j, and ρ is the sand density equivalent to 2650 kg/m^3.

Additionally, assuming that D_{50} is the representative diameter of a particular sand sample, Eq. 1 is converted to Eq. 2 by using $D_{50}^{>210}$ instead of the complete granulometry distribution. Where $D_{50}^{>210}$ corresponds to the median grain diameter of the sample with grains larger than 210 μm ($M^{>210}$) and $\mathrm{EDW}_{D_{50}^{>210}}$ is the respective detection width for the median grain size of the sample $M^{>210}$.

$$\frac{q_{\mathrm{w}_{D_{50}^{>210}}}}{n_{\mathrm{w}}} = \left(\frac{6\, l_{\mathrm{f}}}{\rho \pi (D_{50}^{>210})^3} \left(D_{50}^{>210} + \mathrm{EDW}_{D_{50}^{>210}} \right) \right)^{-1} \tag{2}$$

For all samples, so for each trap and deployment, the grain size distribution was determined by laser diffraction using a Malvern Mastersizer 2000 (Malvern Panalytical Ltd), according to the Fraunhofer diffraction principle (de Boer et al., 1987). Using a Mastersizer, the grain size distribution can be divided up to 100 grain size classes allowing a better

Table 4
Mass(g) of grains larger than 210 μm, obtained from the granulometry of each individual trap.

	Trap 2	Trap 3	Trap 4	Trap 5	Trap 6
Run 1	328.3	71.6	21.1	7.5	2.6
Run 2	416.6	120.5	46.1	18.5	8.8
Run 3	236.3	73.2	26.4	10.5	5.4
Run 4	290.8	90.6	35.6	15.1	7.2
Run 5	500.4	163.1	63.2	26.8	13.9
Run 6	383.6	123.3	53.4	22.7	10.6
Run 7	306.8	103.0	39.3	17.5	9.1
Run 8	411.5	141.6	61.0	27.3	12.7
Run 9	522.7	191.9	75.0	31.4	16.4

Table 5
Mass fluxes ($\times 10^{-3}$, kg/m^{2}s) derived from trap data, considering the proportion of sand with a diameter larger than 210 μm.

	Trap 2	Trap 3	Trap 4	Trap 5	Trap 6
Run 1	33.48	7.30	2.15	0.77	0.26
Run 2	46.24	13.37	5.12	2.05	0.98
Run 3	55.73	17.27	6.23	2.48	1.27
Run 4	62.66	19.52	7.67	3.25	1.56
Run 5	78.69	25.65	9.94	4.22	2.19
Run 6	80.42	25.85	11.19	4.76	2.23
Run 7	48.25	16.19	6.17	2.75	1.42
Run 8	70.59	24.29	10.46	4.69	2.17
Run 9	52.63	19.32	7.55	3.16	1.65

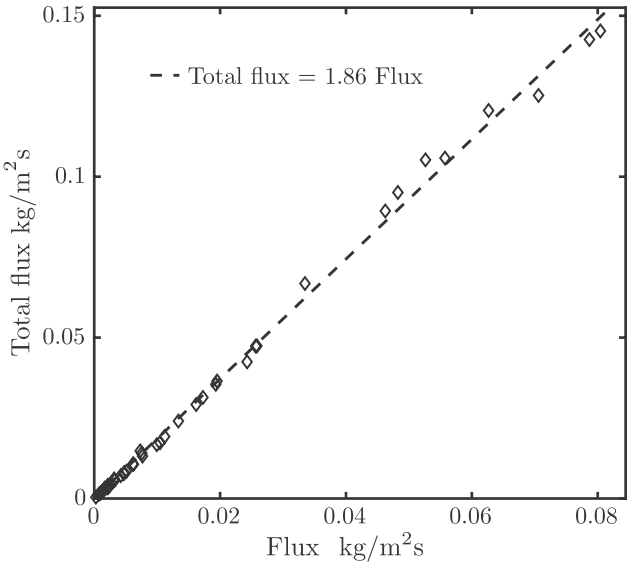

Fig. 4. Total Flux vs Flux from detectable particles (grains larger than 210 μm), for each individual trap during the different runs and the respective regression line.

Table 6
Exponential fit regression coefficients (intercept (α), slope (β), coefficient of determination (R^2) and error sum of squares (SSE)) associated to the vertical mass fluxes for each individual run in Table 5. All the values are related to the geometric center of the traps.

	α (kg/m^{2}s)	β (m^{-1})	R^2	SSE (kg/m^{2}s)^2
Run 1	0.2079	−25.97	0.9975	1.96E-06
Run 2	0.2291	−22.69	0.9987	1.80E-06
Run 3	0.2624	−21.94	0.9994	1.17E-06
Run 4	0.2830	−21.38	0.9988	3.11E-06
Run 5	0.3405	−20.77	0.9991	3.65E-06
Run 6	0.3378	−20.38	0.9980	8.26E-06
Run 7	0.2030	−20.36	0.9992	1.20E-06
Run 8	0.2762	−19.37	0.9985	4.73E-06
Run 9	0.1975	−18.76	0.9997	6.19E-07

estimation of the q_w (Eq. 1). Sperazza et al. (2004) showed that the instrumental precision of the Mastersizer 2000 was ~1% for medium grain sizes, for samples that were measured 15 times without being removed from the instrument.

5. Results

In this section, we compare mass fluxes due to aeolian sand transport derived from Wenglor count data to mass fluxes derived from sand traps. The mass related to the grains larger than 210 μm, $M^{>210}$, for each sand trap during the nine runs is shown in Table 4 (see Appendix, Table A1, for details of the total mass collected in each sand trap during the experiments).

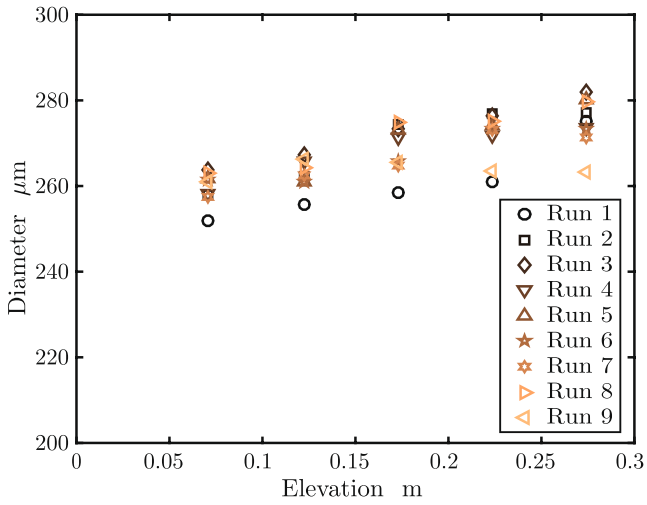

Fig. 5. Mass median particle diameter ($D_{50}^{\geq 210}$), of the detectable part (grains larger than 210 μm), for each sample collected during the different runs.

The calculated fluxes of detectable particles (grains larger than 210 μm), are shown in Table 5. Fig. 4 shows a comparison between Total flux and fluxes associated to the grains larger than 210 μm for each individual sand trap for the several runs. As we can see a linear relationship exists between the total flux and the flux values associated with grains larger than 210 μm. If the Wenglor sensor turns out to be capable of adequately measuring the flux of detectable grain sizes (D>210 μm) in field conditions, this linear relationship demonstrates that the total flux can in principle be inferred from q_w, provided the grain size distribution of transported sediment is known (Eq. 1). The latter is needed because it will provide the information about the proportion of the weight that is in the undetectable grain size range.

Once the fluxes were obtained, an exponential curve was fitted to the vertical distribution of mass flux values, for each of the 9 runs. Table 6 shows the exponential fit regression coefficients, for each of the nine runs. For all the fits the regression coefficient R^2 is larger than 0.99 which is consistent with the statement that the exponential fit is the best way to estimate the vertical flux distribution, as it was shown by Ellis et al. (2009). The differences between the measured and fitted mass flux values, as quantified by the sum of square errors (SSE), amount on average to 15%, being 1% for the bottom trap (sand trap 2) and 20% for the upper ones (sand trap 5 and sand trap 6). In general, the exponential fit underpredicts the measured fluxes for all the sand traps except for sand trap 3. Similar to results presented by Ellis et al. (2009), the regression coefficients, i.e. intercept (α) and slope (β) increase with increasing wind speed (see Table 1) indicating that increasingly more sand is transported at higher elevations above the bed, with increasing wind speed.

Table 7
Time averaged counts/s gathered by each individual Wenglor sensor during the nine runs.

	Wenglor 1	Wenglor 2	Wenglor 3	Wenglor 4	Wenglor 5
Run 1	164	25	25	12	2
Run 2	478	54	62	31	7
Run 3	246	22	14	13	3
Run 4	271	22	10	9	3
Run 5	345	30	14	9	4
Run 6	314	26	11	7	4
Run 7	250	17	6	5	2
Run 8	272	19	7	5	3
Run 9	181	13	5	3	2

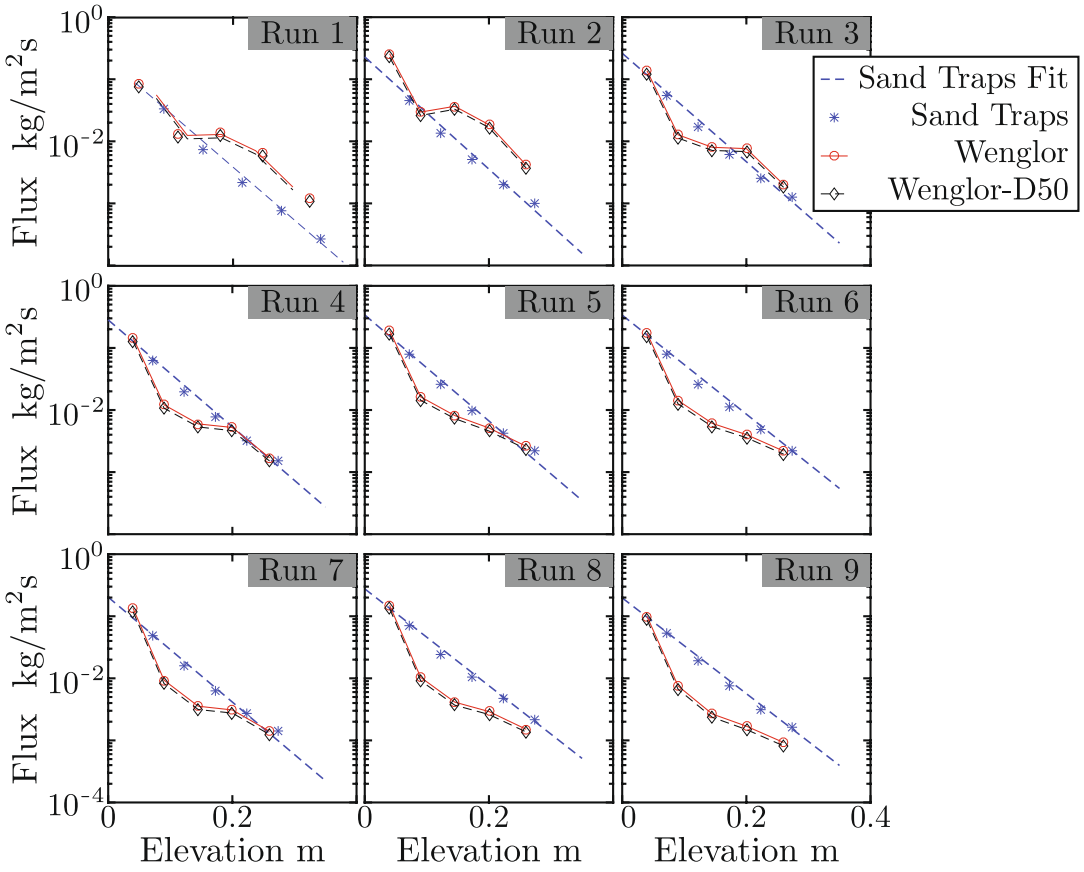

Fig. 6. Vertical distribution of sand transport fluxes for the nine runs. Each subplot includes the fluxes calculated from the trap data, with the exponential regression fit for the vertical array and the fluxes derived from the Wenglor count data, considering the granulometry distribution of grains larger than 210 μm and the $D_{50}^{\geq 210}$ associated to each individual trap during different runs.

Fig. 5 shows the $D_{50}^{\geq 210}$ of each sample presented in Table 4. The values ranged between 252 μm and 282 μm, with an average value of 267 μm and are plotted against the geometric mean elevation (Table 3) of the respective sand trap. As we can see, a slight increase in grain size with height occurs, which is consistent with the conclusions presented by Farrell et al. (2012). If we consider the whole samples of sand collected with our traps, the D50 over all the traps and heights is D50 $=$ 223 $\pm$ 14 μm. For comparison, Strypsteen (2019) obtained a value of D50 $=$ 220 $\pm$ 15 μm, for sand samples collected at the same beach (Koksijde) and on the same day of our experiment, by using Modified Wilson and Cook (MWAC) traps.

Table 7 shows the n_w(counts/s) associated to each individual Wenglor (five elevations) for the nine runs. As expected, the counts/s decrease as the height of the sensor increases.

To calculate the Wenglor fluxes, we considered the granulometry of the sand trap closest to the height of the Wenglor sensor, that is, Wenglor 1 was associated to sand trap 2, Wenglor 2 with sand trap 3 and so on. Fig. 6 shows the fluxes, q_w and $q_{w_{D_{50}^{\geq 210}}}$, obtained according to Eqs. 1 and 2 respectively. The median grain diameters $D_{50}^{\geq 210}$, for every sand trap and run, are the values presented in Fig. 5. Additionally, Fig. 6 also includes the fluxes derived from the traps and their respective exponential fit regression. Using the $D_{50}^{\geq 210}$ instead of the complete granulometry distribution (i.e. for particles larger than 210 μm), the values for $q_{w_{D_{50}^{\geq 210}}}$ do not differ from those from the complete granulometry. Therefore, flux calculations can safely be simplified by using $D_{50}^{\geq 210}$.

Fig. 7 shows a comparison between fluxes derived from sand traps and fluxes calculated from the Wenglor count data for each individual run. The values presented for the sand traps, correspond to the flux obtained from the fitted curve at the elevation of the respective Wenglor. In the first two runs, the fluxes calculated from the upper three Wenglors are considerably larger than the sand trap fluxes (Wenglor 3, Wenglor 4 and Wenglor 5) as is the second run for Wenglor 1.

In particular (Fig. 7), the subplot for Wenglor 1 with sand trap 2 shows a good comparison except during run 2. Wenglors 2 and 3, show a very similar pattern of deviation from their respective trap data, except for run 2. For the Wenglor 4 and 5, both sensors show similar deviation pattern with respect to the trap data, but with two matches during run 4 and run 7. For all the runs, if sand trap flux increases the flux measured with the Wenglor does not necessarily increase in the same proportion (Fig. 8 and Fig. 9).

6. Discussion

Fig. 8 presents the ratio between the derived Wenglor flux and the flux obtained from the sand trap fitted curve at the elevation of the respective Wenglor, for each run and for each Wenglor elevation. The closest match between the fluxes (sand traps and Wenglors) occurred for the sensor 1 and 5, but still with some differences. For all the sensors, the ratio decreases over time. This may be related to an increasing dust build-up on the lens of the Wenglor sensor, which increases the probability of saturation or not detection of grains (Barchyn et al., 2014; Hugenholtz and Barchyn, 2011).

Although dust build-up on the lens might explain some of the differences between the results from Wenglor and sand traps over time, it is still unclear why the Wenglor sensors perform differently. In particular, in run 2, the fluxes derived for Wenglors 1, 3, 4 and 5 are considerably larger than those obtained with the sand traps (see Fig. 7).

Even though the fluxes derived from Wenglors and sand traps are in

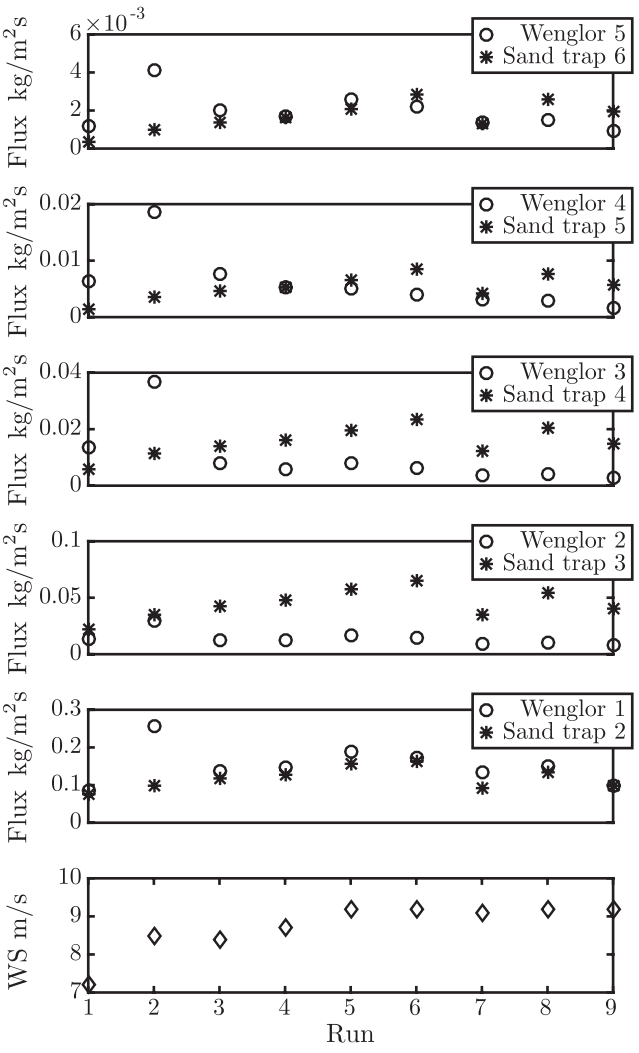

Fig. 7. Sand trap and Wenglor derived fluxes for the nine runs at different elevations. In the bottom subplot, the average wind speed (WS) during each run, at 0.5 m, is shown.

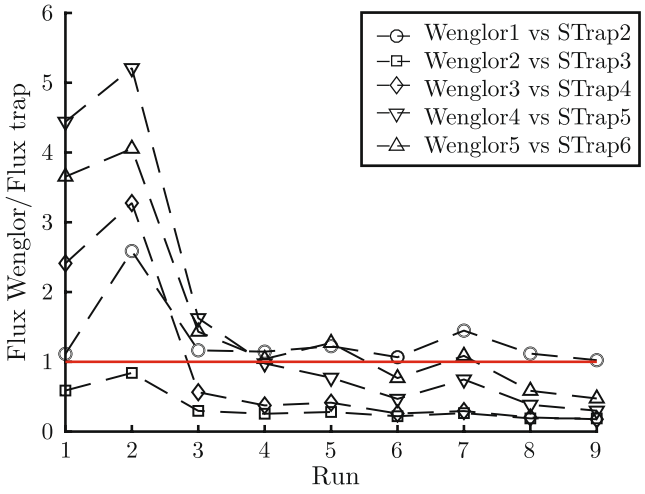

Fig. 8. Ratio between Wenglor and Sand trap derived fluxes for the different runs conducted at the beach. The red line is the boundary between underestimation and overestimation of the fluxes obtained with the Wenglor sensors compared to those obtained with the sand traps.

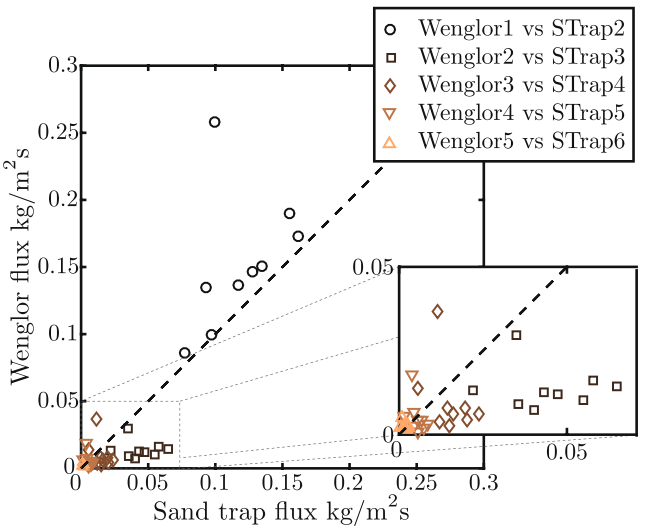

Fig. 9. Comparison between sand trap fluxes and Wenglor fluxes for all the sensors and runs. As in the preceding case, trap fluxes correspond to the values of the fitted curve at the same elevation of the respective Wenglor sensor. The dashed line corresponds to a 1–1 relation and serves as a guide to the eye.

the same order of magnitude and sometimes they are quite similar, and considering only particles above the detection limit (210 μm), still there are significant differences. These differences may be related to sensor saturation or sensor internal processes, as it was discussed in Duarte-Campos et al. (2017).

Another important point is that flux does not represent concentration and therefore, low fluxes values could be related to a high concentration and low wind speed (Hugenholtz and Barchyn, 2011). But, according to our experiments, it seems that the lower sensor –exposed to larger concentrations– has more accuracy if it is compared with the sand transport measured with the sand trap (Fig. 7 and Fig. 9). In this case, Wenglor 1 gives slightly larger fluxes, but this can be explained by the fact that we are ignoring the sand grains smaller than 210 μm, which can be grouped and pass through the laser beam at the same time, creating a "detectable grain" from "invisible particles"; increasing the number of sand grains detected by the Wenglor. For the other Wenglors and sand traps, the mismatch between fluxes can be explained mainly because of a low concentration at elevations more than 10 cm above the surface. The effective area of the sand trap is almost hundred times the Wenglor area and therefore during low particles concentration deployment the Wenglor must be deployed for a longer period of time to have the same chance to be compared with the samples collected by the sand traps. But, the sand trap cannot be deployed for a longer period without losing efficiency.

Martin et al. (2018) presented a methodology to calibrate Wenglors with sand traps, but their calibration parameters show a high variation between sensors, the study area and elevation of the sensor. The difficulties to calibrate the sensor measurements are related to the fact that the particle sizes are too close to the lower limit detection of the sensor. In our case, Fig. 9 shows that is not possible to calibrate all the sensors with only one curve. As we can see, the closest match occurs between Wenglor 1 and sand trap 2, but during the second run a still not fully understood large overestimation in the derived Wenglor fluxes occurred. Due to the large increase in the average wind speed between the first and second run, Wenglor sensors were more exposed to the occurrence of sediment flurries (Bauer and Davidson-Arnott, 2014), which could potentially have increased the number of saturated counts from invisible particles, but is unclear why this did not affect Wenglor 2.

One of the sensor internal processes that may affect the correctness of the count data, hence the accuracy of the derived flux data, is the transformation of the raw analog photoelectric signal into count data.

Using an optical sensor able to deliver an analog photoelectric signal could enrich the data analysis. The results of controlled laboratory experiments conducted by Duarte-Campos et al. (2017), showed that the use of the raw laser intensity signal at the photo sensor of the Wenglor, instead of the binary data output, helped not only in the detection of missed and saturated counts but also in the identification of the minimum intensity reduction to achieve a count. However, recording the analog signal could be challenging during fieldwork experiments due to the huge amount of data generated and its respective data storage required.

Another complicating sensor internal process is the finding that, while it is true that minimum intensity reduction to achieve a count is 18%, a band exists in which the sensor actually can give a count or not. This band covers between 18% and 45% in intensity reduction. These values can be observed in the histograms presented by Duarte-Campos et al. (2017), that show the normalised intensity reduction when a particle passes through the laser beam. A larger minimum intensity reduction means that the minimum detectable grain size will be larger.

An important issue to address, regarding the grain count to flux conversion, is our finding that the quality of Wenglor derived sediment flux values varied by sensor as well as over time for a single sensor, including both under and overestimation of the actual flux values. This makes it a difficult problem to be solved by a calibration approach. Possibly, time varying grain size composition, e.g., in flurries, may also play a role. Etyemezian et al. (2017) presented an in-depth analysis of an optical gate device for measuring aeolian sand transport. Their analysis is useful to understand some of the typical issues that have been observed in deployments of the Wenglor sensor as: saturation, dust build-up in the lens of the sensor or different behaviour between sensors under the same transport conditions. For these measurement problems, they recommend analysing the raw signal from the laser rather than the count data, which is a difficult problem to handle given the current Wenglor sensor design. This would support the recommendation by Martin et al. (2018) to technically improve laser particle counters, to be able to detect airborne particle size distributions at the same time that the sensor counts the particles as happen with snow particle counters (Nishimura and Nemoto, 2005; Leonard et al., 2012; Naaim-Bouvet et al., 2014). Finally, despite the limitations of the Wenglor sensor for quantification of sand fluxes, the sensor could still be useful as a complementary instrument for identification and qualification of the high frequency time-varying aspect of the transport on a fixed height. Further research is suggested to assess whether the high-frequency time varying structure in counts (like the flurries) are consistently observed by multiple Wenglor sensors (co-located in pairs), to learn if time varying structure is more reliably recorded than the actual magnitude of the fluxes.

7. Conclusions

We have presented the results of field experiments to assess the suitability of the Wenglor sensor (YH08PCT8 - 80 mm fork width) for measuring aeolian sand fluxes in field deployments. The Wenglor count data was enriched with grain size information from co-located sand traps. The results show that the fluxes obtained from the vertically stacked mesh sand traps follow an exponential vertical distribution, which did not happen for the Wenglor derived fluxes.

The fact that the Wenglor detects only the coarser portion of the sediment in transport (D>210 μm) does not seem to be a problem. The total flux scaled linearly with the detectable part of the flux, therefore the real challenges are in the correctness of quantifying the detectable part of the sediment flux by the Wenglor. These appeared to be of variable quality, varying between sensors as well as for a single sensor over time. Both over and underestimation of the actual flux values occurred in a manner that seems to be difficult to be solved by calibration. This suggests that further studies using optical aeolian transport sensors should, for instance, take into account the transformation of the raw photoelectric signal to obtain more reliable counting data that can lead to better sediment flux quantification.

Data availability

The data that support the findings of this study are available from the corresponding author on request.

CRediT authorship contribution statement

Leonardo Duarte-Campos: Conceptualization, Data curation, Formal analysis, Investigation, Methodology, Writing - original draft, Writing - review & editing. **Kathelijne M. Wijnberg:** Supervision, Conceptualization, Formal analysis, Investigation, Writing - original draft, Writing - review & editing. **Suzanne J.M.H. Hulscher:** Supervision, Writing - original draft, Writing - review & editing.

Declaration of Competing Interest

The authors declare that they have no known competing financial interests or personal relationships that could have appeared to influence the work reported in this paper.

Acknowledgements

We greatly appreciated the support of Glenn Strypsteen and Pieter Rauwoens (KU Leuven) during the field experiments and for the shared wind data. The authors would like to thank the anonymous reviewers for their comments and suggestions that significantly improved this manuscript. This research was supported by the Becas Chile-CONICYT program.

Appendix

Table A1
Mass (g) captured by each individual trap during every run. For the case of *Run*2 – *Trap*1, the sand sample was not considered due to sand losses during removal process of the mesh bag from the aluminium trap. The numbers in parentheses indicate the bottom and top elevation, in meters, for each sand trap.

	Trap 1 (0.00–0.05)	Trap 2 (0.05–0.10)	Trap 3 (0.10–0.15)	Trap 4 (0.15–0.20)	Trap 1 (0.20–0.25)	Trap 6 (0.25–0.30)
Run 1	1968.0	654.9	145.0	40.1	13.8	4.2
Run 2	–	804.9	216.9	76.0	30.0	14.6
Run 3	1498.4	448.4	133.2	45.1	17.3	9.1
Run 4	1508.0	559.6	169.4	61.2	26.3	12.5
Run 5	2938.4	906.9	301.2	106.4	45.2	22.3
Run 6	2178.6	692.9	226.1	91.8	38.5	18.2
Run 7	2686.8	604.7	185.7	68.4	30.0	16.0
Run 8	2439.2	730.1	247.5	101.0	45.1	20.1
Run 9	3528.6	1045.1	352.4	139.5	60.5	31.9

References

Arens, S., van der Lee, G., 1995. Saltation sand traps for the measurement of aeolian transport into the foredunes. Soil Technol. 8, 61–74.

Baas, A.C., 2004. Evaluation of saltation flux impact responders (safires) for measuring instantaneous aeolian sand transport intensity. Geomorphology 59, 99–118.

Bagnold, R.A., 1936. The Movement of Desert Sand. Proc. R. Soc. A 157, 594–620.

Bagnold, R.A., 1938. The Measurement of Sand Storms. Proc. R. Soc. A 167, 282–291.

Barchyn, T.E., Hugenholtz, C.H., Li, B., Neuman, C.M., Sanderson, R.S., 2014. From particle counts to flux: Wind tunnel testing and calibration of the Wenglor aeolian sediment transport sensor. Aeolian Res. 15, 311–318.

Bauer, B.O., Davidson-Arnott, R.G., Hilton, M.J., Fraser, D., 2018. On the frequency response of a wenglor particle-counting system for aeolian transport measurements. Aeolian Res. 32, 133–140.

Bauer, B.O., Davidson-Arnott, R.G.D., 2014. Aeolian particle flux profiles and transport unsteadiness. J. Geophys. Res.: Earth Surf. 119, 1542–1563.

de Boer, G.B.J., de Weerd, C., Thoenes, D., Goossens, H.W.J., 1987. Laser diffraction spectrometry: Fraunhofer diffraction versus Mie scattering. Part. Part. Syst. Charact. 4, 14–19.

Davidson-Arnott, R.G.D., Bauer, B.O., Walker, I.J., Hesp, P.A., Ollerhead, J., Delgado-Fernandez, I., 2009. Instantaneous and mean aeolian sediment transport rate on beaches: an intercomparison of measurements from two sensor types. J. Coastal Res. S.I. 56, 297–301.

Delgado-Fernandez, I., Davidson-Arnott, R., Bauer, B.O., Walker, I.J., Ollerhead, J., Rhew, H., 2012. Assessing aeolian beach-surface dynamics using a remote sensing approach. Earth Surf. Proc. Land. 37, 1651–1660.

Duarte-Campos, L., Wijnberg, K.M., Oyarte-Gálvez, L., Hulscher, S.J.M.H., 2017. Laser particle counter validation for aeolian sand transport measurements using a highspeed camera. Aeolian Res. 25, 37–44.

Ellis, J.T., Li, B., Farrell, E.J., Sherman, D.J., 2009. Protocols for characterizing aeolian mass-flux profiles. Aeolian Res. 1, 19–26.

Ellis, J.T., Morrison, R.F., Priest, B.H., 2009. Detecting impacts of sand grains with a microphone system in field conditions. Geomorphology 105, 87–94.

Etyemezian, V., Nikolich, G., Nickling, W., King, J.S., Gillies, J.A., 2017. Analysis of an optical gate device for measuring aeolian sand movement. Aeolian Res. 24, 65–79.

Farrell, E., Sherman, D., Ellis, J., Li, B., 2012. Vertical distribution of grain size for wind blown sand. Aeolian Res. 7, 51–61.

Goossens, D., Nolet, C., Etyemezian, V., Duarte-Campos, L., Bakker, G., Riksen, M., 2018. Field testing, comparison, and discussion of five aeolian sand transport measuring devices operating on different measuring principles. Aeolian Res. 32, 1–13.

Goossens, D., Offer, Z., London, G., 2000. Wind tunnel and field calibration of five aeolian sand traps. Geomorphology 35, 233–252.

Haerens, P., Bolle, A., Trouw, K., Houthuys, R., 2012. Definition of storm thresholds for significant morphological change of the sandy beaches along the belgian coastline. Geomorphology 143–144, 104–117.

Hilton, M., Nickling, B., Wakes, S., Sherman, D., Konlechner, T., Jermy, M., Geoghegan, P., 2017. An efficient, self-orienting, vertical-array, sand trap. Aeolian Res. 25, 11–21.

Hoonhout, B., de Vries, S., 2017. Field measurements on spatial variations in aeolian sediment availability at the sand motor mega nourishment. Aeolian Res. 24, 93–104.

Hugenholtz, C.H., Barchyn, T.E., 2011. Laboratory and field performance of a laser particle counter for measuring aeolian sand transport. J. Geophys. Res.: Earth Surf. 116, F01010.

Leatherman, S.P., 1978. A new aeolian sand trap design. Sedimentology 25, 303–306.

Leonard, K.C., Tremblay, L.B., Thom, J.E., MacAyeal, D.R., 2012. Drifting snow threshold measurements near McMurdo station, Antarctica: A sensor comparison study. Cold Reg. Sci. Technol. 70, 71–80.

Martin, R.L., Kok, J.F., Hugenholtz, C.H., Barchyn, T.E., Chamecki, M., Ellis, J.T., 2018. High-frequency measurements of aeolian saltation flux: Field-based methodology and applications. Aeolian Res. 30, 97–114.

Naaim-Bouvet, F., Bellot, H., Nishimura, K., Genthon, C., Palerme, C., Guyomarch, G., Vionnet, V., 2014. Detection of snowfall occurrence during blowing snow events using photoelectric sensors. Cold Reg. Sci. Technol. 106–107, 11–21.

Nishimura, K., Nemoto, M., 2005. Blowing snow at mizuho station, antarctica. Phil. Trans. R. Soc. A 363, 1647–1662.

van Pelt, R.S., Peters, P., Visser, S., 2009. Laboratory wind tunnel testing of three commonly used saltation impact sensors. Aeolian Res. 1, 55–62.

Poortinga, A., van Rheenen, H., Ellis, J.T., Sherman, D.J., 2015. Measuring aeolian sand transport using acoustic sensors. Aeolian Res. 16, 143–151.

Rezaei, M., Goossens, D., Riksen, M.J., 2020. Evaluating the sandflow, an acoustic sediment transport sensor. Aeolian Res. 42, 100558.

Rotnicka, J., 2013. Aeolian vertical mass flux profiles above dry and moist sandy beach surfaces. Geomorphology 187, 27–37.

Sherman, D.J., Li, B., Farrell, E.J., Ellis, J.T., Cox, W.D., Maia, L.P., Sousa, P.H.G.O., 2011. Measuring aeolian saltation: a comparison of sensors. J. Coastal Res. S.I. 59, 280–290.

Sherman, D.J., Swann, C., Barron, J.D., 2014. A high-efficiency, low-cost aeolian sand trap. Aeolian Res. 13, 31–34.

Sperazza, M., Moore, J.N., Hendrix, M.S., 2004. High-Resolution Particle Size Analysis of Naturally Occurring Very Fine-Grained Sediment Through Laser Diffractometry. J. Sediment. Res. 74, 736–743.

Speybroeck, J., Bonte, D., Courtens, W., Gheskiere, T., Grootaert, P., Maelfait, J.P., Provoost, S., Sabbe, K., Stienen, E.W.M., Van Lancker, V., Van Landuyt, W., Vincx, M., Degraer, S., 2008. The Belgian sandy beach ecosystem: a review. Mar. Ecol. 29, 171–185.

Sterk, G., Raats, P.A.C., 1996. Comparison of Models Describing the Vertical Distribution of Wind-Eroded Sediment. Soil Sci. Soc. Am. J. 60, 1914–1919.

Strypsteen, G., 2019. Monitoring and modelling aeolian sand transport at the Belgian coast. Ph.D. thesis. KU Leuven. Belgium.

Strypsteen, G., De Sloover, L., De Wulf, A., Rauwoens, P., 2020. Downwind evolution of aeolian saltation across an artificially constructed coastal berm. Aeolian Res. 47, 100627.

Strypsteen, G., Montreuil, A.L., Rauwoens, P., 2017. Aeolian sand transport at the belgian coast: Field campaigns and first results. In: Proceedings of Coastal Dynamics 2017, pp. 502–512.

Voulgaris, G., Simmonds, D., Michel, D., Howa, H., Collins, M.B., Huntley, D.A., 1998. Measuring and Modelling Sediment Transport on a Macrotidal Ridge and Runnel Beach: An Intercomparison. J. Coastal Res. 14, 315–330.

de Winter, W., van Dam, D., Delbecque, N., Verdoodt, A., Ruessink, B., Sterk, G., 2018. Measuring high spatiotemporal variability in saltation intensity using a low-cost Saltation Detection System: Wind tunnel and field experiments. Aeolian Res. 31, 72–81.

Yurk, B.P., Hansen, E.C., Hazle, D., 2013. A deadtime model for the calibration of impact sensors with an application to a modified miniphone sensor. Aeolian Res. 11, 43–54.